Characterizing and imaging gross and real finger contacts under dynamic loading

Séréna Bochereau, Brygida Dzidek, Michael Adams, and Vincent Hayward, *Fellow, IEEE*

Abstract—We describe an instrument intended to study finger contacts under tangential dynamic loading. This type of loading is relevant to the natural conditions when touch is used to discriminate and identify the properties of the surfaces of objects — it is also crucial during object manipulation. The system comprises a high performance tribometer able to accurately record *in vivo* the components of the interfacial forces when a finger interacts with arbitrary surfaces which is combined with a high-speed, high-definition imaging apparatus. Broadband skin excitation reproducing the dynamic contact loads previously identified can be effected while imaging the contact through a transparent window, thus closely approximating the condition when the skin interacts with a non-transparent surface during sliding. As a preliminary example of the type of phenomenon that can be identified with this apparatus, we show that traction in the range from 10 to 1000 Hz tends to decrease faster with excitation frequency for dry fingers than for moist fingers.

Index Terms—fingerprint imaging, bio-tribology, dynamic loading, tactile stimulation

1 Introduction

For almost a century it has been observed that our tactile system mostly extracts information about the substance and the surface details of objects during the sliding movements of the fingers [1], [2], [3], [4]. Unless a finger contact is nearly perfectly lubricated, the slip of a finger against most surfaces elicits complex oscillations. Steady sliding may occasionally be induced by lubrication from surfactants in aqueous solutions [5], [6], something that happens when we clean dishes with soapy water and experience difficulties feeling them. The more common case of the dry or moderately wet surfaces, however, is invariably associated with slip-induced oscillations.

These perceptually significant mechanical oscillations arise even if the counter-surfaces have roughnesses down to nanometer scales [7]. They are evident for asperities at micrometer scales [8], [9] and higher [10]. These observations justify the need to develop methods to characterise finger contacts under dynamic loading conditions, since such dynamic contacts are the rule rather than the exception during the tactile interaction with objects.

Since the observations of Gibson regarding human perceptual behaviour [11], it has been widely recognised that the information available from statically loading fingers and hands with objects has little perceptual value. There are three main types of informative finger contacts: when a finger interacts with an object causing a quasi-static evolution of its mechanical state, when a finger collides with a surface, and during sliding on a surface or at the onset of slip [12]. Only the latter two cases qualify as dynamic contacts.

The apparatus that was developed in the current work specifically addresses the study of dynamics contacts. The evolution of these contacts can be divided into epochs [13], [14], [15], [16], [7] which typically can be identified through two approaches. A first approach is through the bulk measurement of frictional forces. Such measurements require special instruments owing to the need to obtain a reliable response over a large frequency range, to viz., 500 Hz. A second approach is to image the contact of the finger through a transparent surface. While the bulk frictional response of a finger to movement is relatively easy to obtain in the quasi-static case, the evaluation of the mechanical consequences of the friction associated with a dynamic finger is more difficult. Thus far such characterisation was obtained indirectly, either acoustically [17], through acceleration signals [18], [19], [20], remote velocimetry [10], or directly by imaging through transparent surfaces.

When a person explores a surface, skin tribology depends crucially on the spontaneous motor programs that are called upon for each type of surface and perceptual task. For example, seeking to detect a small asperity on a smooth surface, such as a micro-crack, will involve a very low tonic output, but the identification of the essence of a wood from its grain might evoke much greater activation. Replacing a complex surface with which the skin interacts by a rigid surface that oscillates in a complex manner, [21], is arguably a reasonable approximation to sliding on a complex surface. Consider that the propagation of mechanical waves in the skin is of the order of $10\,\mathrm{m\,s^{-1}}$, [22], which at 10 Hz corresponds to a wavelength of 1 m. At 1 kHz, the wavelength re-

S. Bochereau and V. Hayward are with Sorbonne Universités, UPMC Univ Paris 06, Institut des Systèmes Intelligents et de Robotique, Paris, France, Email: vincent.hayward@isir.upmc.fr.
B. Dzidek and M. Adams are with the school of Chemical Engineering, University of Birmingham, Birmingham, UK
Email: m.j.adams@bham.ac.uk

duces to 10 mm but at such frequencies viscous forces dominate, [23], and the skin may then be considered a rigid solid. It can be further observed through behavioural studies that the tangential component of the interaction force with an object is particularly rich in information concerning the texture roughness and shape of the surface topographical features making up the texture [24].

From the above observations we constructed an apparatus that can excite the skin tangentially with arbitrarily complex displacements in a wide frequency range, while simultaneously imaging the contact at high spatial and temporal resolutions. The apparatus can also measure the tribology of a finger sliding on arbitrary natural surfaces and can further ascertain that interfacial forces, which arise during exploration and during testing, are indeed equivalent. We present preliminary results and discuss their implications. Before doing so, we briefly review relevant contact imaging and tribological measurement techniques.

2 Related Work

2.1 Imaging finger contacts

A prism-based Frustrated Total Internal Reflection principle (FTIR), see Fig. 1, was adopted by Levesque and Hayward to image finger contacts with flat, raised, or indented surfaces [25]. This technique can produce high contrast images of the intimate contact of a finger with a transparent surface. It was possible to image the temporal evolution of the skin strain patterns in the contact region area during rotation and lateral movements. By examining changes in the triangulation of tracked skin features, they found that patterns of skin compression and expansion resulted from a combination of gross movements and surface features.

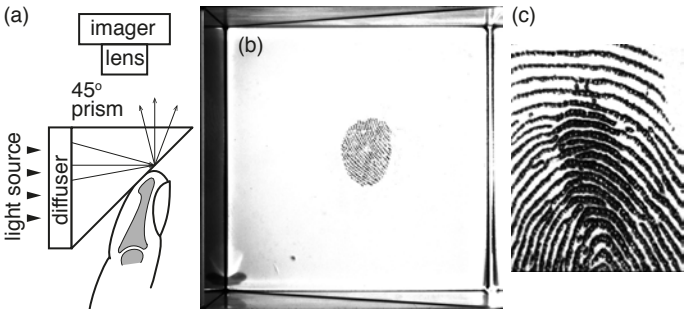

Fig. 1: (a) Prism-based Frustrated Total Internal Reflection principle. With a correctly designed diffuser, light entering the prism is completely reflected, yielding a bright background. Any object in intimate contact (or up to a few tens of nanometers) with the face of the prism at distances smaller than the wavelength of the light disrupts reflection locally. (b) High contrast images of the 'real' contact since objects distant from the surface by more than a few tens of nm will leave reflected light intact. (c) Transitions from sticking to sliding, see [26], can be directly observed since sliding ridges exhibit smaller contacts areas than sticking ridges.

Using the same device, André et al. [15] found that the skin hydration level reduced the tendency of a contact to slip, irrespective of the variations of the coefficient of friction. Delhaye et al. [27], employing a similar technique, but with coaxial illumination to facilitate the movement of the counter-surface, observed the contact area evolution during the stick to slip transition in distal, proximal, radial and ulnar directions. This study examined the differences in the stick ratio and the contact area displacement with time or tangential force using an optical flow algorithm. Coaxial illumination, however, produces lower contrast images than prism-based frustrated reflection since the background inter-ridge surfaces reflect significant light, but it has the advantage of giving images that do not required aspect-ratio correction.

Another very popular approach to take advantage of the Frustrated Total Internal Reflection principle is in a direct manner [28, Sec. 12.3], as shown in Fig. 2(a). Here, light is injected in a slab of glass acting as a light trap, giving a dark background when no object is in contact with it. When there is an intimate contact, reflection is also frustrated, but some of the light escaping from the contact scatters and some diffuses inside the finger tissues. This is due to the fact that the interface surface separating the two light propagating media — the glass and the skin — is discontinuous at many length scales.

The optical effect is a key advantageous property the prism-based FTIR technique owing to its *subtractive* nature, but is a fundamental limitation of the direct approach because the *additive* nature of the process causes a portion of the light to escape from the trap, giving rise to an intensity graded image on a black background Fig. 2(b). Moreover, some of this light reflects from the surfaces that are in close vicinity. In the image shown in Fig. 2(b), the bright spots visible inside the sweat ducts are probably the result of specular reflections of this light against menisci of exuding sweat, see Fig. 2(c). The reflected light is thus modulated by many factors and sweat bridges can be confused with true contact areas. Wiertlewski et al. [29] recently took advantage of this technique for imaging finger contacts at ultrasonic frequencies, which to our knowledge is the first example of *in vivo* finger contact imaging under dynamic loading arising from a moving mechanical boundary.

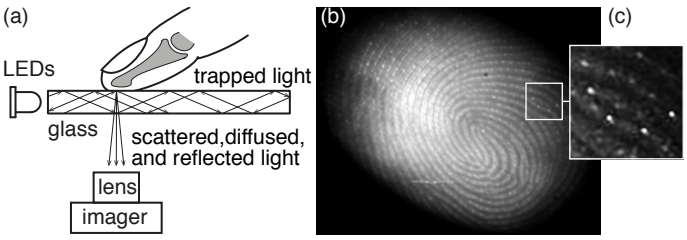

Fig. 2: (a) Imaging finger contacts using frustrated total reflection to scatter light at the points of contact. Illumination can be conveniently provided by LED devices. (b) The resulting image combines scattered, tissue-diffused, and reflected light. (c) Contrast enhanced area of detail shows specularities from sweat menisci.

Lastly, using direct illumination and image processing techniques to compensate for low contrast, Tada and Kanade showed that as the normal force increases, a large overall area is created, and that the stick region disappears faster as speed increases [30].

2.2 Finger Tribometry Against Natural Textures

Several tribometers exist that are capable of measuring finger tribology *in vivo* [31], [32], [33], [34], [35]. Some of these devices are capable of measuring the interaction of a bare finger with a wide range of natural textures [36], [21], [37]. The particular design adopted herein, Fig. 3., was developed by Wiertlweski et al. [38] and adapted by Platkiewicz et al. [39] to record natural textures. Recently, Janko et al. [40] described a high performance tribometer that was employed to identify a range of physical effects arising from the nonlinear nature of friction.

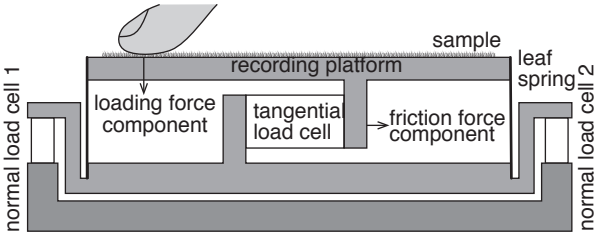

Fig. 3: Tribometer measuring tangential and normal components independently, catering to both the recording (seen here) and the reproduction, seen Fig. 9, apparatuses.

The present design, see Fig. 3, features a very high ratio of interfacial forces component separation to ensure that normal loading and frictional forces are accurately measured. The normal force components was computed using two load cells (9313AA1, Kistler AG, Switzerland) and the tangential force component using one load cell (9217A, Kistler AG, Switzerland). The leaf springs transmitting normal loads to the load cells have the feature of being 1000 times stiffer in the normal direction than in the tangential direction.

3 Device Overview

The device, represented in Fig. 4, consisted of a tribometer that catered to both a recording operating mode and a reproduction/imaging mode. The recording apparatus used a tribometer (a) to record the fluctuating friction force arising between a sample (b) and a sliding finger. These fluctuations could be recreated using an electrodynamic motor (c) and their effect on a finger observed by imaging (d). The recreated forces could be monitored using the same tribometer (a).

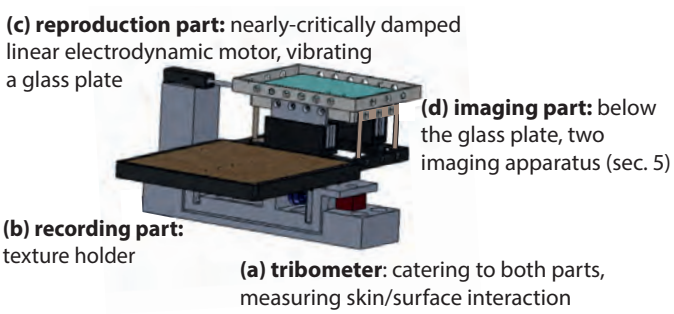

Fig. 4: Device able to record, reproduce and image the fingertip friction elicited when sliding over textures or asperities.

4 Apparatus

4.1 Requirements

The main challenge was to achieve force sensing with sufficient bandwidth, at least up to 500 Hz but ideally up to 1 kHz, in order to cover the temporal frequencies associated with scanning textures [41], [42]. In practice, this requirement reduces down to eliminating any sharply undamped modes from the mechanical structure at frequencies in the desired operating band that would be difficult to compensate by inverse filtering.

In terms of skin excitation, the requirements involved ensuring a stable and robust signal causality relationship between a transducer and a finger over a wide frequency band. One approach, the isotonic approach, is to arrange for the transducer to have a mechanical impedance that is much smaller than that of the finger and to measure displacements resulting from a known applied force. Such an approach is possible, [43], but difficult to implement here owing to the mass of the plate used to image the finger contact. The converse approach, the isometric approach, which is adopted here, is to arrange for the transducer to have an impedance that dominates that of the finger and to measure the force resulting from its displacement.

4.2 Design and Construction

The tribometer design, see Fig. 3, was optimised by constructing it from three single-block mechanical parts connecting the load sensors, achieving high rigidity. The load cells were rigidly attached by fasteners to mechanical parts machined out of single blocks in order to maximise construction rigidity. Next, the sample holder platform was designed to be light and rigid. It was machined out of a single block of grade 2017 aluminium as depicted by Fig. 5.

In the reproduction apparatus, the lateral glass frame supported the skin excitation transducer, which was connected to it by a set of compliant leaf springs. The transducer was actuated by a contactless electrodynamic voice-coil motor (Model NCC01-07-001-1R, H2W, Santa Clarita, CA). It is represented schematically in Fig. 9. The plate in contact with the finger serves as a transparent

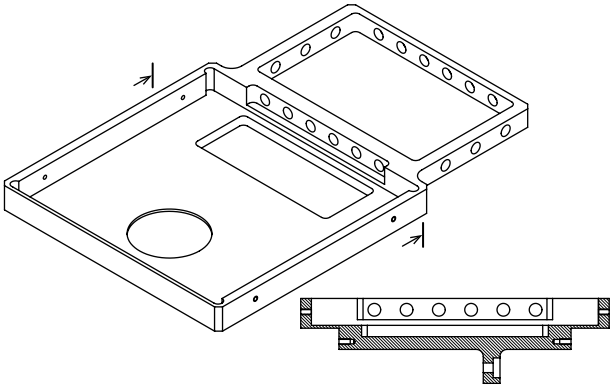

Fig. 5: Sample holder platform. In the recording part, textures samples (10 x 10 cm) can be placed (left) and in the reproduction part, a glass plate (5 x 8 cm) is suspended using leaf springs (right).

imaging window. The imaging system is described in the next section.

The modal response of the sample holder platform was evaluated using an impact hammer to excite the structure (Low impact hammer type 086E80, PCB Piezotronics). The results revealed that the response was satisfactory with a first peak at 550 Hz due to the platform's cantilevered design in order to satisfy the aim of employing the same measurement platform for the recording and the reproduction apparatuses, see Fig. 6. The tribometer's performance was reported in [7].

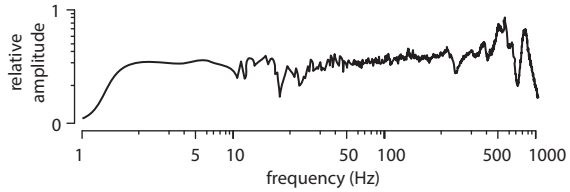

Fig. 6: Mechanical impulse response of the platform over 20 tests.

We adopted the guideline that the stiffness of the plate suspension and the damping coefficient should be of the same order as that of a fingertip while the moving mass should be many times greater in order to achieve the required signal causality. This way, any force applied by the motor to the plate will be converted into an acceleration in a simple manner. In the lateral-medial direction, the mean bulk elasticity of human fingers is known to be about $1.0\,\mathrm{N\,mm^{-1}}$ and the damping coefficient of the order of $1.0\,\mathrm{N\,s\,mm^{-1}}$ [44]. These target figures were thus adopted. As a result of the mechanical properties of the finger, the amplitudes of the bulk oscillations during exploration can reach one or two millimetres, thus the transducer was designed to achieve these values when oscillating at different frequencies.

The springs were made from copper beryllium beams that were cut to give the required stiffness. The frame holding the moving glass plate was machined from magnesium for rigidity and low mass. To achieve the required damping, we designed a Foucault-current damper of a design similar to that described in [45]. The armature was made of two aluminium plates that moved without contact between pairs of magnets, as seen in Fig. 7.

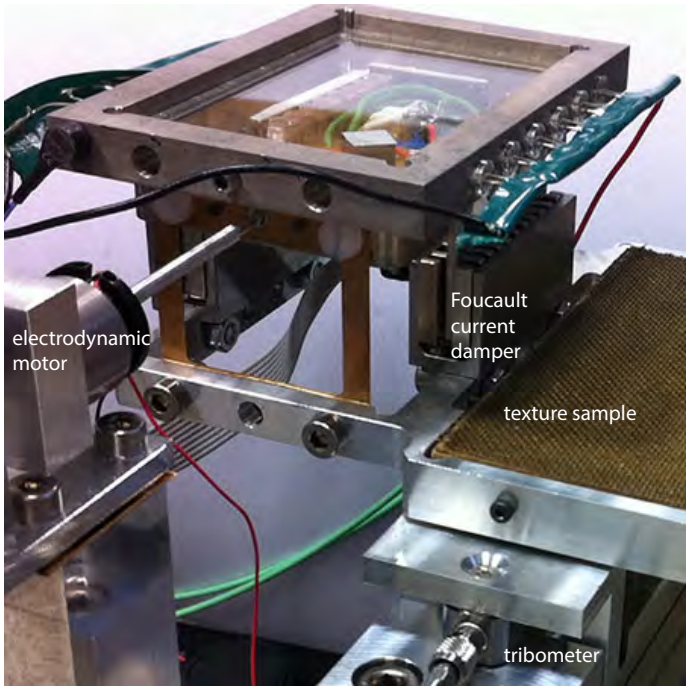

Fig. 7: Reproduction apparatus with transparent platform mounted on the tribometer (left) alongside the recording apparatus where a texture sample is placed (right).

The damping viscosity obtained is a function of several parameters [45]. The size, spacing, and number of magnets are important ones. We employed twelve pairs positioned every 2 mm using plastic spacers on either side of the moving plate. The material with which the armature was made was non-alloyed aluminium (99% pure) to maximise conductivity and minimise mass. The air gap between the magnet and the armature was set to 0.1 mm. The magnets were $15 \times 3.5 \times 2$ mm and made of Neodymium (NdFeB) with nickel coating giving a flux density 1.4 T.

4.3 Identification

Sending a step impulse to the motor, Fig. 8, allowed us to identify the parameters of the system by minimising $|\hat{f}(t) - f(t)|$ where $\hat{f}(t)$ and $f(t)$ are the model and the measured ground reaction forces respectively. To estimate the damping ratio, we fit the response curve to the solution of the governing equation of a forced underdamped system: $f(t) = Ae^{-\xi\omega_0 t}\cos(\omega_d t - \phi)$ where A is the amplitude, ξ the damping ratio, ω_0 the resonance pulsation, w_d the damping pulsation, and ϕ the phase. Identification resulted in the following identified mechanical parameters values: $m = 81\,\mathrm{g}$, $\omega_0 = 17\,\mathrm{Hz}$, $k = 0.93\,\mathrm{N\,mm^{-1}}$, $\xi = 0.35$.

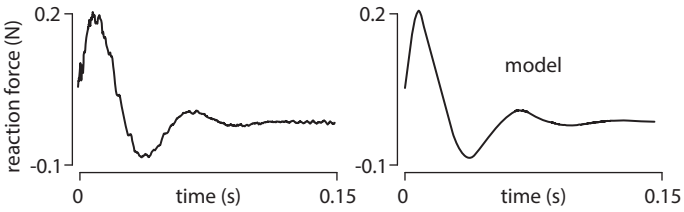

Fig. 8: Damped response to a step function.

4.4 Interfacial force measurement during excitation

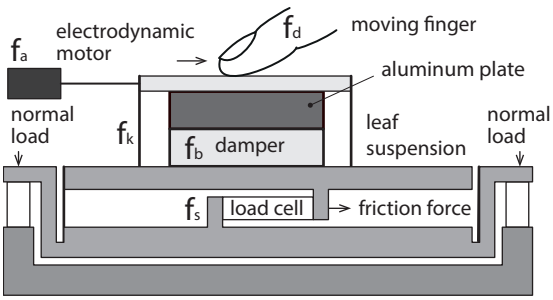

Fig. 9: Reproduction set-up with the sensors to measure a finger-vibrating glass interaction.

From the system's free body diagram, Fig. 9, the forces acting on the plate were: the force of elasticity, f_k, the force of viscosity, f_b, the interfacial force of finger friction, f_d, and the force of the actuators, f_a, giving $-m\ddot{x} = f_k + f_b + f_\mathrm{d} + f_\mathrm{a}$. However, the reaction force sensed by the tribometer's lateral sensor is, $f_\mathrm{s} = f_k + f_b$, thus if the acceleration of the plate, $\ddot{x}$, is measured, then the interfacial force of the finger friction can be evaluated from $f_\mathrm{d} = -m\ddot{x} - f_\mathrm{s} - f_\mathrm{a}$. Thus, we could easily compute f_d since m was known, f_a was precisely controlled, and f_s and $\ddot{x}$ were accurately measured.

4.5 Examples of texture recordings

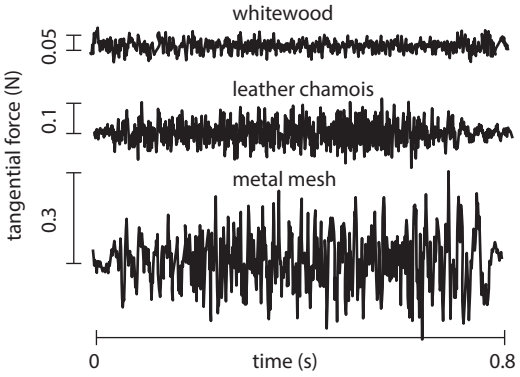

Fig. 10: Friction force measured by the tribometer for three different samples.

Figure 10 shows examples of the difference in information and magnitude obtained in the friction force when a finger was sliding over a metal mesh, chamois leather and whitewood (samples 42, 23 and 111 from [46]) at scanned with a bare finger at roughly 100 mm s^{-1}.

5 Two Imaging apparatuses

A high-speed camera (Model Mikrotron MotionBLITZ EoSens mini2) was employed to image a fingerpad contact under dynamic loading in the two modes described earlier. To achieve high spatial resolution in addition to the high temporal resolution, it was fitted with a Navitar 6000 zoom having a 12 mm fine focus augmented with a telescopic adapter and a 0.75x lens attachement. This set-up allowed focus from a whole fingertip contact down to just five fingerprint ridges at high resolution. Obtaining a sufficient level of illumination was a challenge in order to serve the needs of the two total internal reflection methods that were available. It should be noted that the two imaging techniques employed could not be deployed simultaneously since switching requires re-arrangement and re-calibration.

There are several definitions of the contact area [47]. The gross area, A_gross, corresponds to the overall area that makes up the elliptical shape encompassing the entire contact. With increasing precision, A_ridge excludes the interstitial spaces between the ridges while A_junct is the sum of small segments of the ridges that are in contact with the glass that eventually connect to form A_ridge. Lastly, the real contact area, A_real, is an approximation of the most precise contact area that we are aiming to characterise. There are surface topographical features on the ridges at the length scales of the skin cells and asperities protruding from these cells. Provided that the features are sufficiently compressed under the action of a normal load then is approximately A_junct equal to A_real.

The prism-based method allows us to observe A_junct directly, which is reasonable measure of the real contact area as discussed previously. It allows us to know very precisely the full contact created between the plate and the junctions of the finger pad ridges. Conversely, the direct approach provides an accurate measure of A_gross and leads to some measure of A_ridge. However, it is imprecise due the light being reflected and the sweat may be misinterpreted as *stratum corneum* in contact with the surface, hence the pressure distribution and A_junct cannot be estimated. Instead, its advantage is in providing a representation of the details of the micro-mechanics of the finger pad under different measurement conditions. Calibration of the direct approach is relatively straightforward while the prism-based method requires substantial calibration and adjustment to account for the image distortion.

We achieved an excellent resolution with a pixel size of down to 10 nm. This means that considerable detail of junction contacts with the surface could be resolved in the case of the prism-based technique and how the ridges were shaped and deformed in the case of the direct technique.

5.1 Prism-based Frustrated Total Internal Reflection

A right-angle prism was mounted to a 3-axis micro-positioner that was placed below the vibrating glass

plate and that was adjusted to leave a 0.1 mm gap between the prism and the glass plate. Index-matching immersion oil was then used to fill the gap and the oil was retained there by capillarity, thus realising a continuous, yet deformable, optical milieu, see Fig. 11. A bright cold light source (KL 2500 LED, Schott, Germany) was employed for illumination. An opal diffuser ensured that the light was transmitted onto the camera by illuminating the prism volume without being reflected back by the smooth air-glass interface and without escaping the prism from internal surfaces.

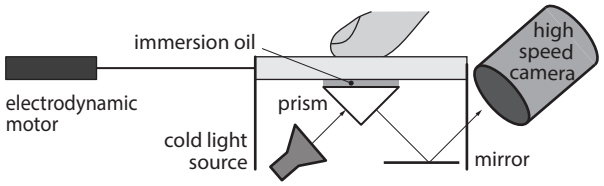

Fig. 11: Dynamically loaded fingertip imaged though prism-based Frustrated Total Internal Reflection set-up.

The prism was immobile, did not add mass to the the moving parts and allowed for high-speed imaging. In this mode, the natural damping introduced by the liquid interfaces eliminated the need for Foucault-current damping. With this technique, images at high spatial resolution and high temporal resolution could be obtained. One example of an image acquired in a static condition is shown in Fig. 12.

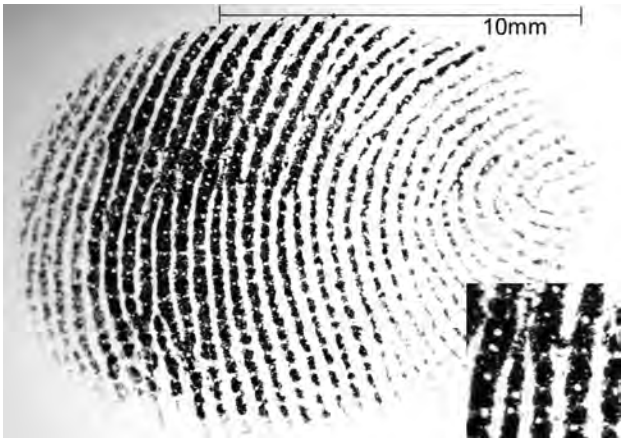

Fig. 12: Occluded real finger contact imaged under static conditions at 24 Hz frame rate showing the degree of detail that can be obtained at 2 N and 2 s of contact time.

Contrast was sufficient to enable excitation at imaging frequencies as high as 1 kHz. One example can be seen in Fig. 13 where a 'real' contact area could easily be imaged at such high frequencies[1].

5.2 Direct Illumination Total Internal Reflection

Green coloured light was transmitted into the glass plate by a set of laterally-placed light emitting diodes (LED),

1. The literature also refers frequently to the notion of 'true' contact. Here the terms 'real' and 'true' are considered to be equivalent.

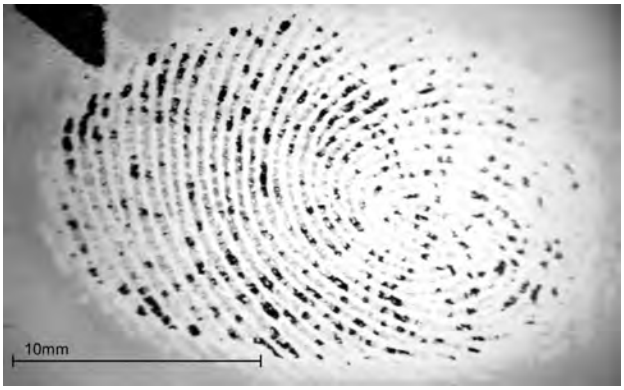

Fig. 13: Real finger contact area under static conditions at a 1 kHz frame rate after 2 s of contact time and for a 2 N normal load.

creating total internal reflection, and allowing for the fingerprint in contact with the plate to be visible. To increase light incidence, the four edges of the glass plate were polished to an optical quality finish. The green coloured light minimised the fraction of light diffused by the skin tissue, which acted as a filter for the complementary colour.

The frame was designed to house twelve green LEDs (HLMP-CM1A-560DD, Avago, 59 000 mcd each) with 15° dispertion giving 36 lm of illumination in total. They shone through 2 mm diaphragms to guide as much light as possible into the 2 mm-thick glass plate to reduce the reflections on the edges of the glass that could escape the light trap, see Fig. 14. Optionally to increase the light intensity even further, we also used a cold light source (KL 2500 LED, Schott, Germany) with a green filter transmitting the light into the glass frame. With this configuration, it was possible to reach 100 Hz image sampling capability.

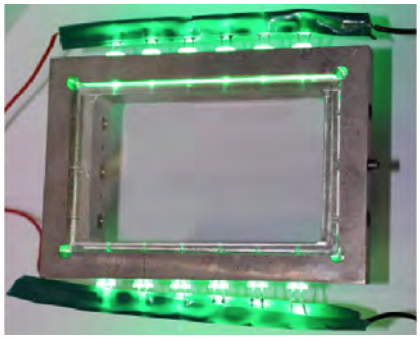

Fig. 14: Illuminated vibrating plate.

A 45° angle mirror was used to enhance the optical stability of the set-up and facilitate the horizontal camera mounting, see Fig. 15. The light path from the green LEDs around the set up was frustrated until light reflected off a fingerprint ridge in contact with the glass.

Figure 16 illustrates the type of image that can be obtained with this method. It is a combination of light

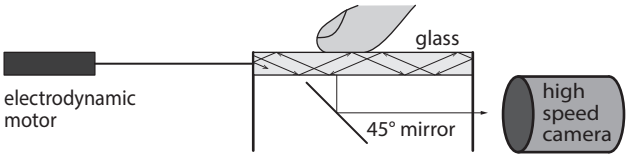

Fig. 15: Direct Frustrated Total Internal Reflection set-up.

arising from the real contact, light reflected by the fingerpad surface, and light diffused in the tissue. This image should be contrasted with that seen in Fig. 13 as they each deliver very different types of information.

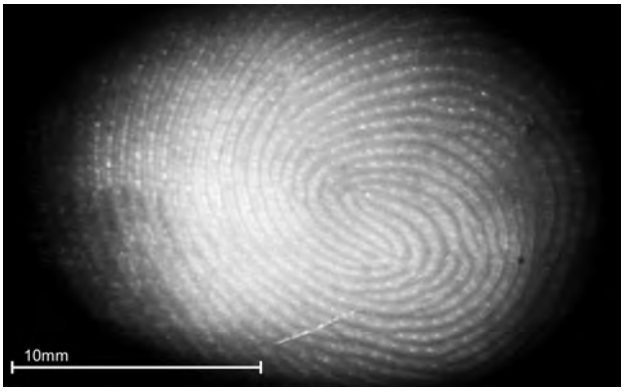

Fig. 16: Fingerpad image mode at 100 Hz for 2 N normal load.

One could wonder by how much the ridge deform and whether the skin is soft enough to be flattened at the molecular level. The topography of every ridge is different, making answering this question difficult. With sweat accumulation, the highest and most rounded ridges become softer and flatten faster, while some ridges are already flattened and yet others will never be fully flattened owing to their geometry.

6 Preliminary bio-tribology measurements

In this section we show some examples of the stimulation and characterisation capabilities of the apparatus described previously. It is made evident without elaborative quantification that the establishment of the real contact area by a finger is a multifactorial phenomenon. For brevity, the physics behind these observations will be discussed in future publications.

6.1 Real Contact Area Dynamics during Static Loading

The imaging apparatus was able to precisely visualise the way in which the real contact area evolves with occlusion time and with applied load, see [26] and [35], for a definition of these terms. Briefly, occlusion occurs when a fingerpad is in contact with a smooth impermeable surface so that the secretion of moisture from the sweat pores in the fingerprint ridges is trapped at the interface and is absorbed by the *stratum corneum*. The ridges and their surface topographical features become more compliant over a period of tens of seconds due to the plasticisation by the moisture and hence the real area of contact increases with the time of contact until an asymptotic value is reached.

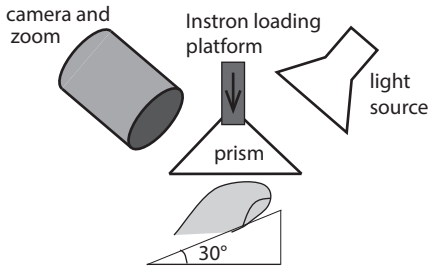

Fig. 17: Imaging apparatus where a glass prism is pressed down onto a static finger pad, used for static loading tests.

A static test was performed while the real finger contact area was imaged in a time-lapsed manner using the prism-based FTIR method, (1, 1.5, 3, 5, 8, and 20 s). A flat glass prism was pressed down onto the fingerpad at a gradual constant loading rate until reaching approximately 2 N in order to induce total internal reflection, with the applied load gradually increased until the required maximum value is achieved. We observed this phenomenon previously using a different apparatus configuration [35], see Fig. 17. Before a set of measurements, the index finger was washed with commercial soap, rinsed with distilled water and allowed to dry for 10 min until an equilibrated clean skin state was achieved. The glass plate was cleaned before each trial with optical wipes in order to remove the sweat that was secreted by the finger pad during the previous trial. Ordinary flat glass was used in all the experiments. They had hydrophilic properties since no treatment or coating was applied. The result can be seen in Fig. 18.

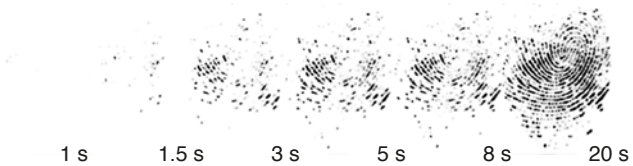

Fig. 18: Time-lapse real contact imaging as the normal load increases according to the time dependent normal loading indicated by Fig. 19.

It can be observed how the real contact area increases gradually owing to occlusion dynamics while the gross contact area reaches its ultimate value very rapidly, see Fig. 19. This phenomenon was discussed and analysed elsewhere in greater detail where the methods are also described [47].

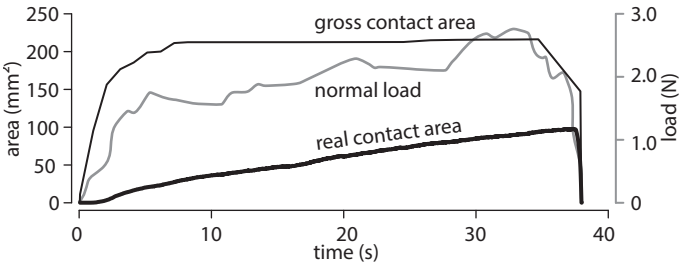

Fig. 19: Result of the analysis of the images of Fig. 18.

6.2 Real Contact Area Under Dynamic Conditions

Exploring textures always corresponds to dynamic contacts since fingertips constantly make and break multiple contacts as the skin ridges interact with the relatively moving asperities. It is these rapid mechanical fluctuations that contain the texture perceptual information.

During steady sliding, the resulting broadband, complex oscillations that can be readily observed and converted to the frequency domain and thus viewed as a sum of a large number of sinusoidal signals. It is thus informative to investigate how dynamic contacts behave as a function of frequency. The formation of the real contact area as the origin of friction between a fingertip and a surface is a multifactorial phenomenon. To investigate these factors, dynamic tests were performed where the participant pressed a finger on the glass plate, and then maintained it at around 1 N while the plate was vibrated at different frequencies. Absence of slip between the fingerpad and the glass plate could be visually ascertained. The same fingerpad skin state preparation was carried out for the dynamic conditions as for the static ones. Figure 20 illustrates the complex influence of the different factors that were varied: tangential loading rate, contact duration, and skin hydration.

Several trends can be observed by simple inspection. Skin hydration has a significant impact at the onset of a contact and during its evolution, as can be observed by comparing images (row pairs) taken for the same loading conditions but at different times after contact onset. Dry and moist refer to different natural states of the finger; the index finger of one of the authors was cleaned at the beginning of the block of trial, then dabbed with either a dry or moist tissue before each measurement to induce the appropriate state. She was a 27 years old and gave her informed consent to perform the experiment. The effects of dynamic lateral loading are also different according to normal loading rate as can be seen by inspection of the columns of Fig. 20.

Notably, a moist finger tended to become less sensitive to loading rate than a dry finger. Another trend is that dynamic normal loading does not seem to disrupt the occlusion process and hence the increase in the real area of contact with time. Since finger hydration could not be controlled with accuracy, monotonicity is not always present in the images sequences taken under different conditions. Taking advantage of the simultaneous tribological measurement, we could nevertheless conduct a preliminary quantification of the creation of traction for different hydration states under dynamic loading.

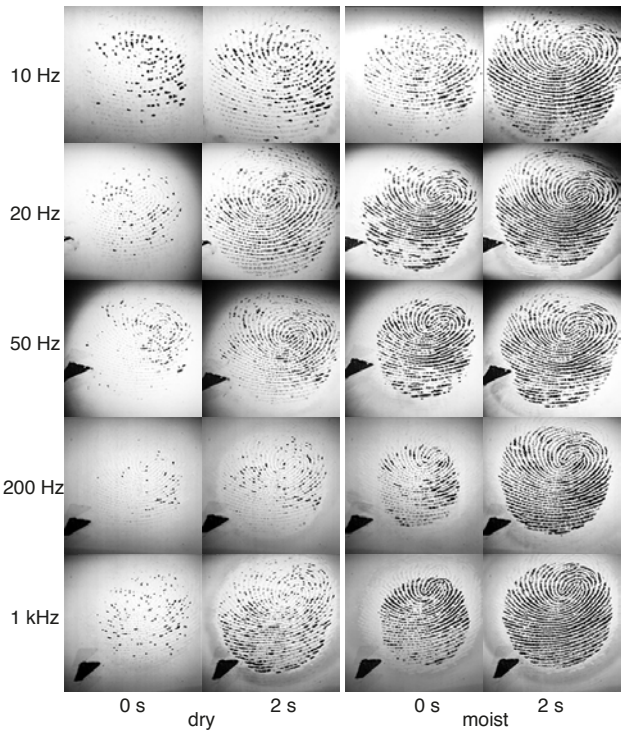

Fig. 20: Real contact imaging as a function of tangential loading rate, contact duration, and skin hydration.

Figure 21 reports the resulting traction measured under the above conditions and at frequencies of 10, 20, 50, 100, 200, 500, and 1000 Hz. At each frequency, the plate vibrated at a similar amplitude of a few millimetres. Recall that traction, or interfacial shear stress, is defined as the force per unit of real contact area [26]. In this preliminary analysis we averaged the tangential traction force component and the real contact area over three trials per condition of duration 2.0 s. The normal load was (0.94 ± 0.60) N for the dry condition and (0.75 ± 0.30) N for the moist condition. To minimise the estimation error of the real contact area due to the variations in the initial moisture contents, the value employed in the analysis was based on the difference between the final and initial values.

The interfacial shear strength is in the range from 0 to 1.2 MPa and this is considerable greater than the values of $\sim$5 kPa reported for the *stratum corneum* of the inner forearm [34], but in this latter case the skin was equilibrated with water in the contact region. The data in Fig. 21 correspond to fingerprint ridges being exposed to a limited amount of moisture from the secretion of sweat for a period of only 2 s and thus the compliance of the *stratum corneum* would be significantly less than when fully hydrated. Based on some complex contact mechanics modelling, it has been argued that a single value of 115 MPa is sufficient to rationalise the frictional behaviour of both dry and wet wrist skin [48]. However,

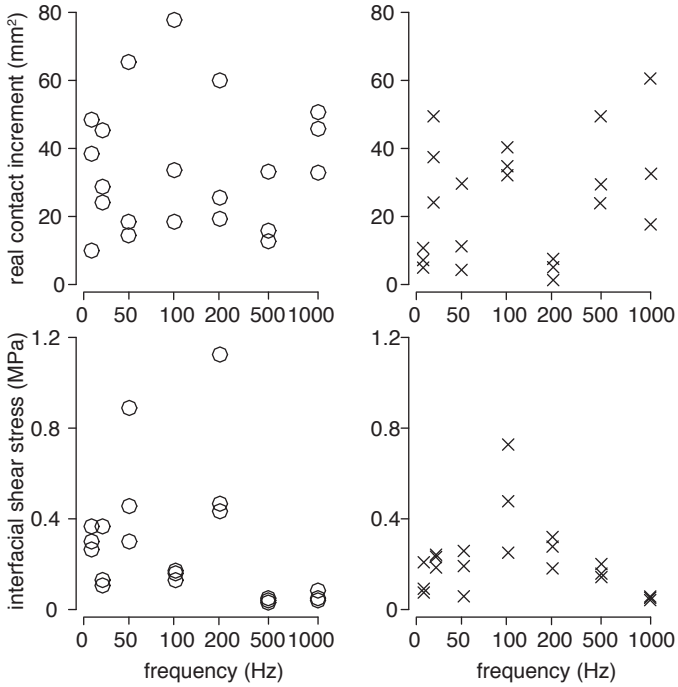

Fig. 21: Real contact growth over 2 s and interfacial shear stress as a function of tangential loading frequency (○ dry, × moist).

it was calculated that the ratio of the real area of contact to the gross value was only 6.59×10^{-4} for wet skin unless it was assumed that capillary forces acted at asperity contacts. The small fractional area could have arisen from assuming that the Youngs modulus of stratum corneum in the wet state is ∼7 MPa since recently it was shown that the value for the fingerprint ridges in the fully occluded state is ∼0.1 MPa [49]. Moreover, for the inner forearm measurements [34], since the frictional force tended to zero when the applied normal force was zero, capillary forces would have been negligible compared to the applied values.

It can be observed that while the formation of the real contact area (as measured by the real contact increment in Fig. 21, which is equivalent to the difference in the contact area between 0 and 2 s in Fig. 20 for each test), is relatively insensitive to loading rate, interfacial shear stress (tangential force/contact area increment) tends to decrease with this parameter. This effect is less pronounced for moist fingers than for dry fingers since there are more consistently lower values than 0.4 MPa for the moist condition. A possible explanation for this phenomenon can be found in the acceleration of the occlusion mechanism at the low frequencies, resulting from an observed more distinct compression and decompression of the fingerprint ridges thus increasing sweat secretion. Thus the effect is weaker at higher frequencies for dry fingers since moisture results in a contact with a significant initial occlusion [47]. Note that the estimation of interfacial shear stress accounted only for the increment of real contact area over a period of 2 s. The observation that the growth of real contact area for dry fingers is more sensitive to the effect of time, and here to loading rate, than it is for moist fingers may contribute to explaining the previously observed phenomenon that the dryness of fingers may not necessarily impact significantly on the coefficient of friction but rather the propensity of a finger contact to fail rapidly under load [15].

6.3 Images obtained with direct FTIR

Images taken under direct FTIR were acquired in conditions similar to that of the previous section but for lower frequencies and longer durations owing to the limitations of this approach in obtaining contrasted images. Unlike those of Fig. 20, the frames shown in Fig. 22 were heavily processed to compensate for the lack of illumination dynamics by normalising them to the darkest and brightest pixels. This means that the images obtained at the onset of a contact have very few brightness levels.

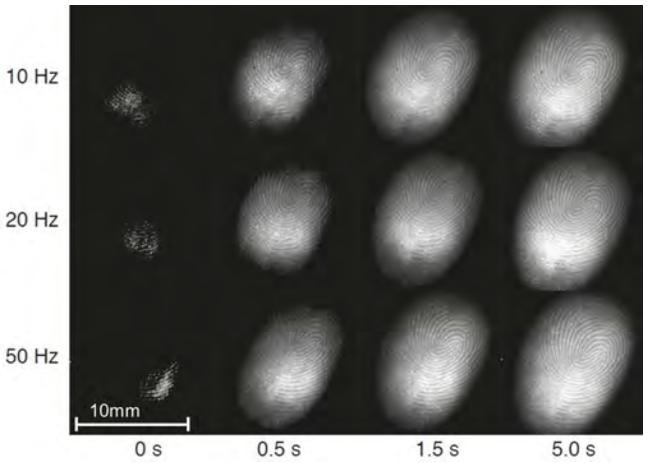

Fig. 22: Images acquired using direct FTIR.

The comparison of the images in Fig. 20 and in Fig. 22 strongly corroborates the measurements computed in [29] that the brightness level strongly correlates with friction, which is turn is correlated with the real contact area. In effect its real contact is likely to increase the portion of light being scattered while the other contributors to brightness, diffusion and reflection, would remain by and large unchanged. On the other hand, the notion that brightness correlates with the mean contact pressure is not well supported by the present results since correlating brightness, and hence real contact, with gross pressure would depend on an analysis of the contact mechanics at the ridge length-scale and more importantly at the asperity length-scale [47].

7 Conclusion

We described an apparatus capable of recording the dynamics of finger interaction with natural textures and to excite fingers with the same dynamics but with the added benefit of imaging with high spatial and temporal

resolutions the evolution of both the gross behaviour of the finger through direct FTIR as well as the microscopic details of the real contact area. This will allow us to gain information on how a fingerpad deforms under load while sliding on otherwise non-transparent materials.

The apparatus enables a wide range of studies related to physical underpinning of tactile material discrimination and identification in perceptual tasks. It could also lead to a better understanding of the grip regulation mechanisms on arbitrary surfaces.

Standardised loading patterns such as sharp transients or step loadings can also be examined in order to visualise the transient phenomena that most certainly take place during natural discriminative or prehensile behaviours. The role of the fingerprint in tactile perception may also potentially be clarified since our newly introduced technique will allow us to investigate the behaviour of ridges at frequencies that are relevant to natural conditions. Future work may also involve evaluating the effects of dynamic loading on fingertip ridge deformation.

ACKNOWLEDGMENT

This work was supported by the FP7 Marie Curie Initial Training Network PROTOTOUCH, (No. 317100) and the European Research Council (FP7) ERC Advanced Grant (PATCH) to V.H. (No. 247300). The authors would like to thank Ramakanth Singal, Bernard Javot, and Rafał Pijewski for excellent engineering advice, Stephen Sinclair for invaluable help with the signal acquisition software, and Simon Johnson for great advice regarding the imaging apparatus.

REFERENCES

[1] L. E. Krueger, "Tactual perception in historical perspective: David Katz's world of touch," in *Tactual Perception; A Sourcebook*, W. Schiff and E. Foulke, Eds. Cambridge University Press, 1982, pp. 1–55.

[2] S. J. Lederman and R. L. Klatzky, "Extracting object properties through haptic exploration," *Acta Psychol.*, vol. 84, no. 1, pp. 29–40, 1993.

[3] M. Hollins, R. Faldowski, S. Rao, and F. Young, "Perceptual dimensions of tactile surface texture: A multidimensional scaling analysis," *Percept. Psychophys.*, vol. 54, no. 6, pp. 697–705, 1993.

[4] M. Hollins and S. J. Bensmaïa, "The coding of roughness," *Can. J. Exp. Psychol.*, vol. 61, no. 3, pp. 184–195, 2007.

[5] S. C. Richards and A. D. Roberts, "Boundary lubrication of rubber by aqueous surfactant," *J. Phys. D: Appl. Phys.*, vol. 25, no. 1A, p. A76, 1992.

[6] W. H. Briscoe, S. Titmuss, F. Tiberg, R. K. Thomas, D. J. McGillivray, and J. Klein, "Boundary lubrication under water," *Nature*, vol. 444, no. 7116, pp. 191–194, 2006.

[7] D. Gueorguiev, S. Bochereau, A. Mouraux, V. Hayward, and J.-L. Thonnard, "Touch uses frictional cues to discriminate flat materials," *Sci. Rep.*, vol. 6, p. 25553, 2016.

[8] M. Wiertlewski, C. Hudin, and V. Hayward, "On the 1/f noise and non-integer harmonic decay of the interaction of a finger sliding on flat and sinusoidal surfaces," in *Conf. Proc. World Haptics*, 2011, pp. 25–30.

[9] E. Wandersman, R. Candelier, G. Debrégeas, and A. Prévost., "Texture-induced modulations of friction force: the fingerprint effect," *Phys. Rev. Lett.*, vol. 107, no. 16, p. 64301, 2011.

[10] L. R. Manfredi, H. P. Saal, K. J. Brown, M. C. Zielinski, J. F. Dammann, V. S. Polashock, and S. J. Bensmaia, "Natural scenes in tactile texture," *J. Neurophysiol.*, vol. 111, no. 9, pp. 1792–1802, 2014.

[11] J. J. Gibson, "Observations on active touch," *Physiol. Rev.*, vol. 69, pp. 477–491, 1962.

[12] V. Hayward, "Is there a plenhaptic function?" *Philos. Trans. R. Soc. Lond. B*, vol. 366, no. 1581, pp. 3115–3122, 2011.

[13] E. R. Serina, C. D. Mote Jr., and D. Rempel, "Force response of the fingertip pulp to repeated compression - effects of loading rate, loading angle and anthropometry," *J Biomech.*, vol. 30, pp. 1035–1040, 1997.

[14] D. T. V. Pawluk and R. D. Howe, "Dynamic lumped element response of the human fingerpad," *J Biomech. Eng.*, vol. 121, no. 2, pp. 178–183, 1999.

[15] T. André, V. Levésque, V. Hayward, P. Lefèvre, and J.-L. Thonnard, "Effect of skin hydration on the dynamics of fingertip gripping contact," *J. R. Soc. Interface.*, vol. 8, no. 2, pp. 1574–1583, 2011.

[16] A. V. Terekhov and V. Hayward, "Minimal adhesion surfaces in tangentially loaded digital contacts," *J. Biomech.*, vol. 44, no. 13, pp. 2508–2510, 2011.

[17] F. Martinot, P. Plenacoste, and C. Chaillou, "Haptic sounds and vibrations of human fingerprints," in *Int. Conf. on Sensing Tecnology.*, 2005, pp. 615–620.

[18] T. Iwamoto and H. Shinoda, "Finger ring tactile interface based on propagating elastic waves on human fingers," in *Conf. Proc. World Haptics*, 2007, pp. 145–150.

[19] Y. Tanaka, Y. Horita, A. Sano, , and H. Fujimoto, "Tactile sensing utilizing human tactile perception," in *Conf. Proc. World Haptics*, 2011, pp. 621–626.

[20] Y. Shao, V. Hayward, and Y. Visell, "Spatial patterns of cutaneous vibration during whole-hand haptic interactions," *PNAS*, vol. 113, no. 15, pp. 4188–4193, 2016.

[21] M. Wiertlewski, J. Lozada, and V. Hayward, "The spatial spectrum of tangential skin displacement can encode tactual texture," *IEEE Trans. Robot.*, vol. 27, no. 3, pp. 461–472, 2011.

[22] R. O. Potts, E. M. Buras, and D. A. Chrisman, "Changes with age in the moisture content of human skin," *J. Invest. Dermatol.*, vol. 82, no. 1, pp. 97–100, 1984.

[23] Q. Wang and V. Hayward, "Biomechanically optimized distributed tactile transducer based on lateral skin deformation," *Int. J. Robot. Res.*, vol. 29, no. 4, pp. 323–335, 2010.

[24] A. M. Smith, C. E. Chapman, M. Deslandes, J. S. Langlais, and M. P. Thibodeau, "Role of friction and tangential force variation in the subjective scaling of tactile roughness," *Exp. Brain Res.*, vol. 144, no. 2, pp. 211–223, 2002.

[25] V. Levesque and V. Hayward, "Experimental evidence of lateral skin strain during tactile exploration," in *Conf. Proc. Eurohaptics*, 2003, pp. 261–275.

[26] M. J. Adams, S. A. Johnson, P. Lefèvre, V. Lévesque, V. Hayward, T. André, and J.-L. Thonnard, "Finger pad friction and its role in grip and touch," *J. R. Soc. Interface.*, vol. 10, no. 80, p. 20120467, 2013.

[27] B. Delhaye, P. Lefèvre, and J.-L. Thonnard, "Dynamics of fingertip contact during the onset of tangential slip," *J. R. Soc. Interface.*, vol. 11, no. 100, p. 0698, 2014.

[28] R. Ehrlich, *Why toast lands jelly-side down: Zen and the art of physics demonstrations*. Princeton University Press, 1997.

[29] M. Wiertlewski, R. F. Friesen, and J. E. Colgate, "Partial squeeze film levitation modulates fingertip friction," *PNAS*, vol. 113, no. 33, pp. 9210–9215, 2016.

[30] M. Tada and T. Kanade, "An imaging system of incipient slip for modelling how human perceives slip of a fingertip," in *Conf. Proc. IEEE Eng. Med. Biol. Soc.*, 2004, pp. 2045–2048.

[31] S. Pasumarty, S. Johnson, S. Watson, and M. J. Adams, "Friction of the human finger pad: Influence of moisture, occlusion and velocity," *Tribol. Lett.*, vol. 44, no. 2, pp. 117–137, 2011.

[32] F. Massi, E. Vittecoq, E. Chatelet, A. Saulot, and Y. Berthier, "Design of a tribometer for investigating tactile perception," *Proc. Inst. Mech. Eng. J J. Eng. Tribol.*, vol. January, 2014.

[33] S. Derler and L.-C. Gerhardt, "Tribology of skin: Review and analysis of experimental results for the friction coefficient of human skin," *Tribol. Lett.*, vol. 45, no. 1, pp. 1–27, 2012.

[34] M. Adams, B. Briscoe, and S. Johnson, "Friction and lubrication of the human skin," *Tribol. Lett.*, vol. 26, no. 3, pp. 239–253, 2007.

[35] B. Dzidek, M. Adams, Z. Zhang, S. Johnson, S. Bochereau, and V. Hayward, "Role of occlusion in non-coulombic slip of the finger pad," in *Haptics: Neuroscience, Devices, Modeling, and Applications, Part-I*, 2014, pp. 109–116.
[36] A. H. F. Martinot and M. C. C. Biet, "Mechanical responses of the fingerpad and distal phalanx to friction of a grooved surface: Effect of the contact angle," *IEEE Trans. Haptics*, pp. 297–300, 2006.
[37] T. A. Fishel and G. E. Loeb., "Bayesian exploration for intelligent identication of textures," *Front. Neurorobot.*, vol. 6, pp. 17 603–17 611, 2012.
[38] M. Wiertlewski, S. Endo, A. M. Wing, and V. Hayward, "Slip-induced vibration influences the grip reflex: A pilot study," in *Conf. Proc. World Haptics*, 2013, pp. 627–632.
[39] J. Platkiewicz, J. Mansutti, A. Bordegoni, and V. Hayward, "Recording device for natural haptic textures felt with the bare fingertip," in *Haptics: Neuroscience, Devices, Modeling, and Applications, Part-I*, 2014, pp. 521–528.
[40] M. Janko, R. Primerano, and Y. Visell, "On frictional forces between the finger and a textured surface during active touch," *IEEE Trans. Haptics*, vol. 9, no. 2, pp. 221–232, 2015.
[41] A. W. Goodwin and J. W. Morley, "Sinusoidal movement of a grating across the monkey's fingerpad: Representation of grating and movement features in afferent fiber responses," *J. Neurosci.*, vol. 7, no. 7, p. 2168, 1987.
[42] G. Campion and V. Hayward, "Fundamental limits in the rendering of virtual haptic textures," in *Conf. Proc. World Haptics*, 2005, pp. 263–270.
[43] M. Wiertlewski and V. Hayward, "Transducer for mechanical impedance testing over a wide frequency range through active feedback," *Rev. Sci. Instrum.*, vol. 83, no. 2, p. 025001, 2012.
[44] ——, "Mechanical behavior of the fingertip in the range of frequencies and displacements relevant to touch," *J Biomech.*, vol. 45, no. 11, pp. 1869–1874, 2012.
[45] A. Mohand-Ousaid, G. Millet, S. Regnier, S. Haliyo, and V. Hayward, "Haptic interface transparency achieved through viscous coupling," *Int. J. Robot. Res.*, vol. 31, no. 3, pp. 319–329, 2012.
[46] W. M. B. Tiest and A. M. Kappers, "Analysis of haptic perception of materials by multidimensional scaling and physical measurements of roughness and compressibility," *Acta Psychol.*, vol. 121, no. 1, pp. 1–20, 2005.
[47] B. Dzidek, S. Bochereau, M. Adams, V. Hayward, and S. Johnson., "Frictional dynamics of finger pads are governed by four length-scales and two time-scales," in *Proc. Haptic Symposium*, 2016, pp. 161–166.
[48] B. N. J. Persson, A. Kovalev, and S. N. Gorb, "Contact mechanics and friction on dry and wet human skin." *Tribol. Lett.*, vol. 50, no. 1, pp. 17–30, 2013.
[49] B. M. Dzidek, M. J. Adams, J. A. Andrews, Z. Zhang, and S. A. Johnson, "Contact mechanics of the human finger pad under compressive loads," *J. R. Soc. Interface*, vol. 14, no. 127, 2017.

Séréna Bochereau received an MEng in Materials Science from the University of Oxford in 2013. She is currently a Marie Curie PhD Fellow at the Institut des Systèmes Intelligents et de Robotique at Université Pierre et Marie Curie, Paris. Her current research include physical invariants in tactile perception and the reproduction of natural textures.

Brygida Dzidek received her Master Degree in Material Science Engineering at University of Silesia in Poland. Specialised in smart biomaterials systems. The objectives of her PhD research are experimental and analytical analysis of tribological interaction of the finger pad and tactile displays.

Mike Adams (FREng, FIChemE, FInstP, FRSC) joined the University of Birmingham School of Chemical Engineering in 2004 as Professor of Product Engineering and Manufacture from Unilever R&D where he was a Senior Scientist with responsibilities for materials science and product processing. In 1999, he was awarded the Donald Julius Groen Prize by the Institution of Mechanical Engineers for outstanding achievements in the tribology of complex materials and in 2016 he was awarded the Tribology Trust Silver Medal for outstanding and sustained contributions to the science and technology of Tribology. He has published over 200 scientific papers and co-edited four books on Tribology in Particulate Technology, Theoretical and Computational Methods in Tribology, Solid-Solid Interactions and Dynamics of Complex Fluids. His research interests include the tribology of skin and the finger pad. He has coordinated a number of EU projects on tactile sensors and haptic displays.

Vincent Hayward (M'84-SM'04-FIEEE'08), Dr-Ing degree in 1981 from the University de Paris XI. He was a postdoctoral fellow then a visiting assistant professor in 1982 at Purdue University, and joined CNRS, France, as Chargé de Recherches in 1983. In 1989, he joined the Department of Electrical and Computer Engineering at McGill University as an assistant, associate, and then a full professor in 2006. He is now professor at the Université Pierre et Marie Curie. He has published more than 250 articles in journals and conferences, co-founded spin-off companies and received best paper and research awards. He was on the editorial boards of the IEEE Transactions on Robotics, the ACM Transaction on Applied Perception, and the IEEE Transactions on Haptics.